

THE SUPERNOVA THAT DESTROYED A PROTOGALAXY: PROMPT CHEMICAL ENRICHMENT AND SUPERMASSIVE BLACK HOLE GROWTH

DANIEL J. WHALEN^{1,2}, JARRETT L. JOHNSON¹, JOSEPH SMIDT¹, AVERY MEIKSIN³, ALEXANDER HEGER⁴, WESLEY EVEN⁵
AND CHRIS L. FRYER⁵

Draft version April 23, 2021

ABSTRACT

The first primitive galaxies formed from accretion and mergers by $z \sim 15$, and were primarily responsible for cosmological reionization and the chemical enrichment of the early cosmos. But a few of these galaxies may have formed in the presence of strong Lyman-Werner UV fluxes that sterilized them of H_2 , preventing them from forming stars or expelling heavy elements into the IGM prior to assembly. At masses of $10^8 M_\odot$ and virial temperatures of 10^4 K, these halos began to rapidly cool by atomic lines, perhaps forming $10^4 - 10^6 M_\odot$ Pop III stars and, later, the seeds of supermassive black holes. We have modeled the explosion of a supermassive Pop III star in the dense core of a line-cooled protogalaxy with the ZEUS-MP code. We find that the supernova (SN) expands to a radius of ~ 1 kpc, briefly engulfing the entire galaxy, but then collapses back into the potential well of the dark matter. fallback fully mixes the interior of the protogalaxy with metals, igniting a violent starburst and fueling the rapid growth of a massive black hole at its center. The starburst would populate the protogalaxy with stars in greater numbers and at higher metallicities than in more slowly-evolving, nearby halos. The SN remnant becomes a strong synchrotron source that can be observed with eVLA and eMERLIN and has a unique signature that easily distinguishes it from less energetic SN remnants. Such explosions, and their attendant starbursts, may well have marked the birthplaces of supermassive black holes on the sky.

Subject headings: early universe – galaxies: high-redshift – galaxies: quasars: general – stars: early-type – supernovae: general – radiative transfer – hydrodynamics – black hole physics – accretion – cosmology:theory

1. INTRODUCTION

After the appearance of the first stars ended the cosmic Dark Ages at $z \sim 25$ (Bromm et al. 1999; Abel et al. 2000, 2002; Bromm et al. 2002; Nakamura & Umemura 2001; O’Shea & Norman 2007, 2008; Wise & Abel 2007; Yoshida et al. 2008; Turk et al. 2009; Stacy et al. 2010; Clark et al. 2011; Smith et al. 2011; Greif et al. 2011, 2012), primeval galaxies formed by accretion and mergers between cosmological halos by $z \sim 15$ (Johnson et al. 2008; Greif et al. 2008; Johnson et al. 2009; Greif et al. 2010; Jeon et al. 2012; Pawlik et al. 2011; Wise et al. 2012; Pawlik et al. 2013). Radiation and strong winds from these galaxies began to reionize (Whalen et al. 2004; Kitayama et al. 2004; Alvarez et al. 2006; Abel et al. 2007; Wise & Abel 2008) and chemically enrich the IGM (Mackey et al. 2003; Smith & Sigurdsson 2007; Smith et al. 2009; Joggerst et al. 2010; Joggerst & Whalen 2011; Ritter et al. 2012; Chiaki et al. 2013).

A few of these galaxies form in the vicinity of strong sources of Lyman-Werner (LW) UV flux that sterilize

them of H_2 , preventing them from cooling and forming primordial stars or hosting SN explosions prior to assembly (e.g., Johnson et al. 2012a). These protogalaxies reach masses of $10^8 M_\odot$ and virial temperatures of 10^4 K without having blown any gas into the IGM or been chemically enriched. At 10^4 K, gas in these halos began to cool by H lines, triggering catastrophic baryon collapse at their centers with infall rates of up to $1 M_\odot \text{yr}^{-1}$ (Wise et al. 2008; Regan & Haehnelt 2009; Shang et al. 2010; Wolcott-Green et al. 2011). These rates are 1000 times those that created the first stars and may have led to the formation of supermassive gas fragments.

In most cases these fragments bypassed star formation and collapsed directly to $10^4 - 10^5 M_\odot$ black holes (BHs). These objects may have been the progenitors of the supermassive black holes (SMBHs) found in most massive galaxies today (Bromm & Loeb 2003; Begelman et al. 2006; Johnson & Bromm 2007; Djorgovski et al. 2008; Lippai et al. 2009; Tanaka & Haiman 2009; Pan et al. 2012b). The creation of SMBH seeds by direct baryon collapse is favored by many because it is difficult for the BHs of Population (Pop) III stars to sustain the rapid growth needed at early times to reach $10^9 M_\odot$ by $z \sim 7$ (Fan et al. 2003; Willott et al. 2003; Fan et al. 2006; Milosavljević et al. 2009; Alvarez et al. 2009; Park & Ricotti 2011; Mortlock et al. 2011; Park & Ricotti 2012a; Whalen & Fryer 2012; Park & Ricotti 2012b; Johnson et al. 2012b). It was originally believed that LW fluxes capable of fully quenching Pop III star formation were rare, and that this might explain why only \sim one $10^9 M_\odot$ BH is

¹ T-2, Los Alamos National Laboratory, Los Alamos, NM 87545

² Universität Heidelberg, Zentrum für Astronomie, Institut für Theoretische Astrophysik, Albert-Ueberle-Str. 2, 69120 Heidelberg, Germany

³ Institute for Astronomy, University of Edinburgh, Blackford Hill, Edinburgh EH9 3HJ, UK

⁴ Monash Centre for Astrophysics, Monash University, Victoria, 3800, Australia

⁵ CCS-2, Los Alamos National Laboratory, Los Alamos, NM 87545

found per Gpc^{-3} at $z \sim 7$, but it has recently been discovered that such conditions may have been far more common in the early universe than previously thought (Dijkstra et al. 2008; Johnson et al. 2012a; Agarwal et al. 2012; Petri et al. 2012).

Some supermassive clumps in line-cooled halos formed stable stars instead of collapsing directly to BHs (Iben 1963; Fowler & Hoyle 1964; Fowler 1966; Appenzeller & Fricke 1972a,b; Bond et al. 1984; Fuller et al. 1986; Begelman 2010). It is now known that some of these stars died in the most energetic thermonuclear explosions in the universe (Montero et al. 2012; Heger & Chen 2013). Recent simulations have shown that such SNe will be visible in both deep-field and all-sky NIR surveys at $z \gtrsim 10$ by the *James Webb Space Telescope (JWST)* and the Wide-Field Infrared Survey Telescope (WFIRST) and Wide-Field Imaging Surveyor for High-Redshift (WISH) (Whalen et al. 2012b) (see also Scannapieco et al. 2005; Fryer et al. 2010; Kasen et al. 2011; Pan et al. 2012a; Hummel et al. 2012; Dessart et al. 2013; Whalen et al. 2013b, 2012a,c, 2013a; de Souza et al. 2013, for other work on Pop III SN light curves). The effects of a $55,500 M_{\odot}$ thermonuclear SN on a protogalaxy and its surrounding cosmological flows has just been studied by Johnson et al. (2013b). For explosions in low ambient densities, like those of an H II region formed by the star, they found that the SN blows most of the baryons from the protogalaxy to radii of $\gtrsim 10$ kpc, or about ten times the virial radius of the halo. Some of this gas, which is heavily enriched by metals from the SN, later falls back into the halo on timescales of 100 Myr.

However, past work has shown that many supermassive Pop III stars may not form H II regions because of the enormous infall rates at the centers of line-cooled halos (Johnson et al. 2012a). The star may then have exploded in very high ambient densities capable of radiating away most of the energy of the SN as bremsstrahlung x-rays in very short times, before the ejecta can be blown from the halo (Kitayama & Yoshida 2005; Whalen et al. 2008) (see also Vasiliev et al. 2012, for studies of less massive SNe in early protogalaxies). This perhaps more likely scenario could not be studied by Johnson et al. (2013b) because such losses occur on scales of 0.001 - 10 pc, below the resolution limit of their GADGET (Springel et al. 2001; Springel & Hernquist 2002) simulation. In very dense environments it is not clear if any of the ejecta escapes the halo. If not, fallback in the dark matter (DM) potential of the halo could be enormous, mixing vigorously with the gas and causing it to cool and fragment into new stars. Fallback could also drive super-Eddington accretion in black holes formed by other massive fragments in the halo, causing them to grow at much higher rates than in the absence of an explosion.

We have now modeled supermassive Pop III SNe in such environments with the ZEUS-MP code. Our simulations bridge all relevant scales of the flow, 0.001 pc to 10 kpc. We describe our numerical method in Section 2. The energetics and hydrodynamics of the SNe are examined in Section 3, and we calculate the radio signatures of the remnant in Section 4. The implications of our results for the fossil chemical abundance record, starbursts in early protogalaxies, and SMBH seed growth are discussed in Section 5.

2. NUMERICAL METHOD

We consider explosions in the dense cores of two protogalaxies: the $4 \times 10^7 M_{\odot}$ atomically-cooled halo from GADGET in Johnson et al. (2013b) and a 3.2×10^8 line-cooled halo evolved from cosmological initial conditions with the *Enzo* code. This mass range brackets those with which LW protogalaxies are expected to form at $z \sim 15$. The evolution of the SN in spherically-averaged density profiles for these halos is then modeled with ZEUS-MP (Whalen & Norman 2006, 2008b,a). As in Whalen et al. (2008), we evolve the SNe on expanding grids in the DM potential of the protogalaxy. Hydrodynamics and nine-species non-equilibrium H and He gas chemistry are solved self-consistently to capture the energetics of the SN remnant. As a fiducial case, we examine the dynamics and energetics of the supermassive SN in the GADGET halo in detail.

2.1. Protogalaxy Models / Halo Profiles

The simulation details for our GADGET halo are described in Johnson et al. (2011); here, we discuss the *Enzo* model of our more massive protogalaxy. *Enzo* (O’Shea et al. 2004) is an adaptive mesh refinement (AMR) cosmology code. It utilizes an N -body adaptive particle-mesh scheme (Efstathiou et al. 1985; Couchman 1991; Bryan & Norman 1997) to evolve DM and a piecewise-parabolic method for fluid dynamics (Woodward & Colella 1984; Bryan et al. 1995). A low-viscosity Riemann solver for is used for capturing shocks, and in these runs we use the recently implemented HLLC Riemann solver (Toro et al. 1994) for enhanced stability for strong shocks and rarefaction waves.

Like ZEUS-MP, *Enzo* solves nine-species H and He gas chemistry and cooling together with hydrodynamics (Abel et al. 1997; Anninos et al. 1997). To approximate the formation of a protogalaxy in a strong LW background, we evolve the halo with H_2 cooling turned off for simplicity. We initialize our simulation volume with gaussian primordial density fluctuations at $z = 150$ with MUSIC (Hahn & Abel 2011), with cosmological parameters from the seven-year *Wilkinson Microwave Anisotropy Probe (WMAP)* $\Lambda\text{CDM}+\text{SZ}+\text{LENS}$ best fit (Komatsu et al. 2011): $\Omega_{\text{M}} = 0.266$, $\Omega_{\Lambda} = 0.734$, $\Omega_{\text{b}} = 0.0449$, $h = 0.71$, $\sigma_8 = 0.81$, and $n = 0.963$.

To capture an atomically-cooled halo in a mass range of $10^8 - 10^9 M_{\odot}$ by $z \sim 15$, we use a 2 Mpc simulation box with a resolution of 1024^3 . This yields DM and baryon mass resolutions of 59.7 and $11.6 h^{-1} M_{\odot}$ respectively. We use a maximum refinement level $l = 13$, and refine the grid on baryon overdensities of $3 \times 2^{-0.2l}$. We also refine on a DM overdensity of 3 and resolve the local Jeans length with at least four zones at all times to avoid artificial fragmentation during collapse (Truelove et al. 1997). If any of these three criteria are met in a given cell, the cell is flagged for further refinement. We show an image of the protogalaxy at $z = 15.3$ in Fig. 1. At this redshift it has reached a mass of $3.2 \times 10^8 M_{\odot}$ and is about to merge with another halo, as shown in the right panel of Fig. 1.

The spherically-averaged density profile of the GAD-

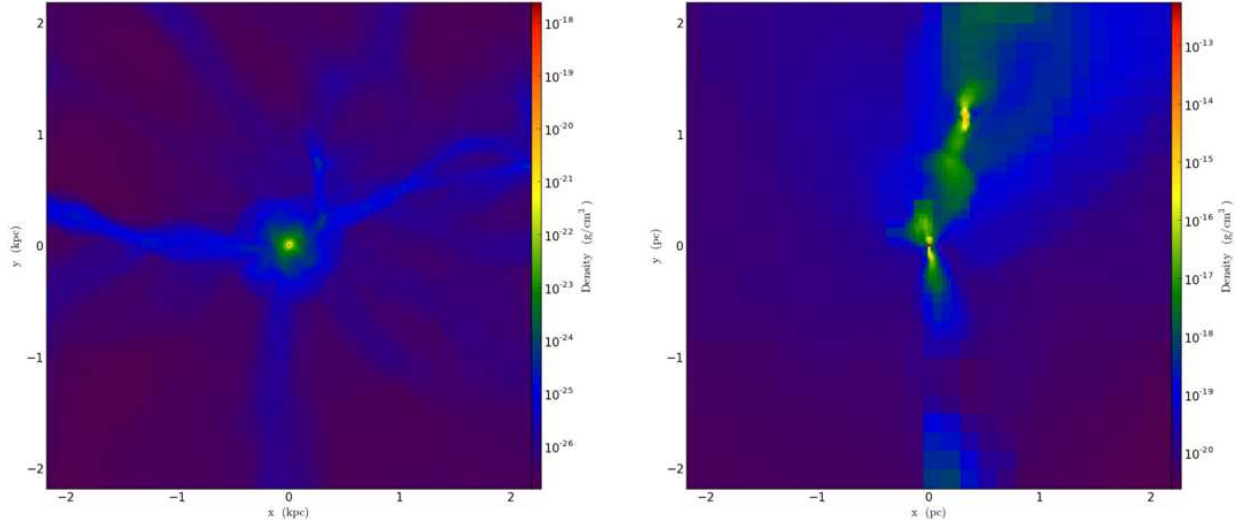


FIG. 1.— Projections of the $3.2 \times 10^8 M_{\odot}$ line-cooled protogalaxy formed by *Enzo* at $z = 15.3$. Left: 1 kpc scale. Right: 1 pc scale. Note that a second halo is about to merge with the more massive protogalaxy on the right.

GET halo is well approximated by

$$n(r) = 10^3 \left(\frac{r}{10 \text{ pc}} \right)^{-2} \text{ cm}^{-3}. \quad (1)$$

The density profile of the more massive protogalaxy evolved in *Enzo*, together with our fit for this halo, are shown in Fig. 2. We find that it is fit well by

$$n(r) = 6417.1 \left(\frac{r}{10 \text{ pc}} \right)^{-2.2} \text{ cm}^{-3}. \quad (2)$$

The density peak at ~ 1 pc in the *Enzo* profile is due to the smaller halo that is about to merge with the protogalaxy in the right panel of Fig. 1. It is not included in Eq. 2 because it presents a relatively small solid angle to the oncoming shock and will not affect its overall dynamics. We take the gas velocities of both halos to be zero for simplicity, their temperatures to be 8500 K (GADGET) and 12,000 K (*Enzo*), and their mass fractions to be 76% H and 24% He.

2.2. SN Blast Profiles

Our initial blast profile is the 10^{55} erg thermonuclear SN of a $55,500 M_{\odot}$ star from Whalen et al. (2013a) (see also Heger & Chen 2013). The explosion was evolved in the *Kepler* and RAGE codes (Weaver et al. 1978; Woosley et al. 2002; Gittings et al. 2008; Frey et al. 2013) out to 2.9×10^6 s, after breakout from the star but well before it has swept up its own mass. The SN ejects $23,000 M_{\odot}$ of metals (and perhaps molecules and dust; Cherchneff & Lilly 2008; Cherchneff & Dwek 2009, 2010; Dwek & Cherchneff 2011; Gall et al. 2011) into the IGM. At this stage it is a free expansion, and its potential energy is a small fraction of its total energy so it is not necessary to account for its self gravity. We show profiles for the explosion in Fig. 3. Densities, velocities and internal energies from RAGE are mapped onto a uniform

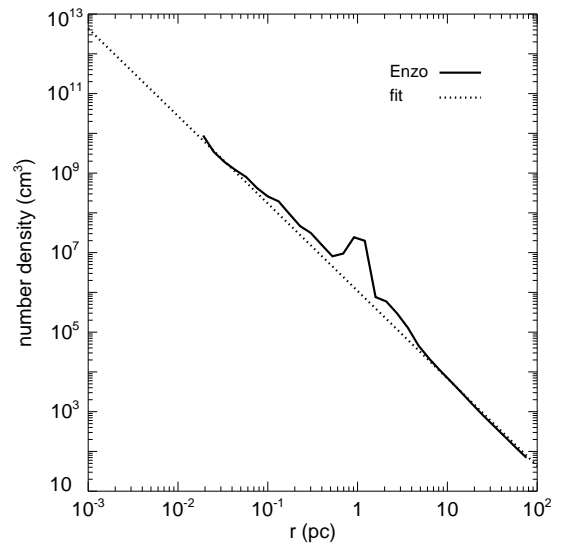


FIG. 2.— Spherically-averaged baryon density profile for the $3.2 \times 10^8 M_{\odot}$ protogalaxy evolved in *Enzo* together with our fit to this halo given by Equation 2. Note that the subsidiary halo in the right panel of Fig. 1, which is about to merge with the protogalaxy and appears in the profile as the bump in density at ~ 1 pc, is excluded from our fit.

one-dimensional (1D) spherical polar coordinate grid in ZEUS-MP using a simple linear interpolation of the logarithm of the quantity versus log radius. The radius of the shock is 3.9×10^{15} cm and the inner and outer grid boundaries are zero and 5.0×10^{15} cm, respectively. The coordinate mesh has 250 zones.

2.3. Nonequilibrium H/He Gas Chemistry

We evolve H, H^+ , He, He^+ , He^{++} , H^- , H_2^+ , H_2 , and e^- with the thirty-reaction rate network described in Anninos et al. (1997) in order to tally energy losses in the shock as it sweeps up and heats baryons. Cooling by collisional excitation and ionization of H and He, recom-

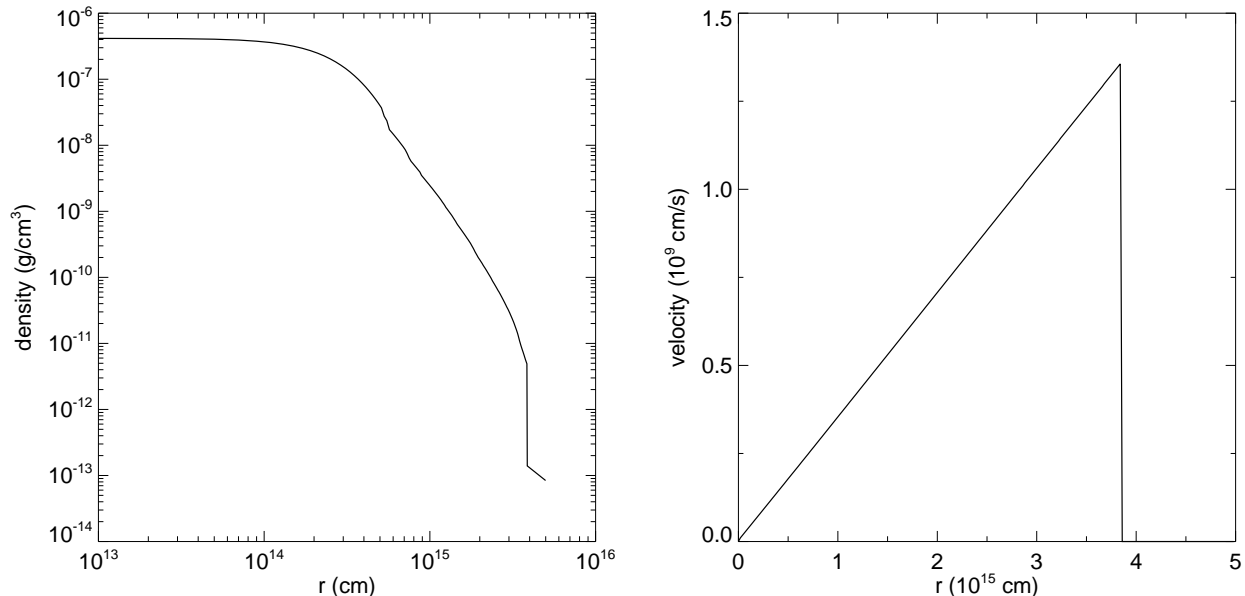


FIG. 3.— Profiles for the supermassive Pop III SN and the surrounding halo as initialized in ZEUS-MP. Left: densities; right: velocities. The r^{-2} density envelope of the protogalaxy (for the case of no H II region) is visible beyond the shock. At this stage, the SN is a free expansion.

binations, inverse Compton (IC) scattering from the cosmic microwave background (CMB), and free-free emission by bremsstrahlung x-rays are included. The rates at which these processes occur depend on the chemical species in the shocked gas, which in turn are governed by the reaction network. We exclude H_2 cooling because high temperatures destroy these fragile molecules in the shock. At early stages of the explosion we also deactivate H and He line cooling because x-rays from the shock ionize these species in the swept-up gas. These cooling channels are switched on when the shock temperature falls to 10^6 K.

2.4. Static DM Potential

Rather than spherically-averaging the DM distribution of the protogalaxy in GADGET and mapping its gravitational potential into ZEUS-MP, we simply take its potential to be that required to keep the density profile in Equation (1) in hydrostatic equilibrium on the grid. The mass associated with this potential is nearly identical to that of the halo. We interpolate this precomputed potential onto the grid at the beginning of the run and onto each new grid thereafter, but the potential itself never evolves. Assuming the potential to be static is an approximation because unlike the models of Whalen et al. (2008), dynamical times for supermassive SNe in protogalaxies are comparable to merger and accretion timescales in the protogalaxy. It has also been shown that Pop III SNe in halos with DM cusps can alter the structure of the cusp (de Souza et al. 2011), and hence the potentials in which they themselves evolve.

2.5. Expanding Grid

When the shock reaches a predetermined distance from the outer edge of the grid, a new grid is created and densities, velocities, energies and species mass fractions for the flow are mapped onto it. The ambient density of the halo,

which is precomputed in a table that is binned by radius, is imposed on the expanding flow as time-dependent updates to the outer boundary conditions. The density that is assigned to the outer boundary is interpolated from the tabled values bracketing the radial bin into which the grid boundary falls at the given time step. This density then migrates inward toward the shock over time as it is mapped onto the grid at greater and greater distances from the outer boundary in subsequent regrids. In this manner the shock always encounters the proper halo densities as it grows by many orders of magnitude in radius. At the beginning of a run we allocate the first 80% of the grid to the SN profile and the remainder to the surrounding halo.

A new grid is calculated when the shock crosses into the outer 10% of the current mesh. At a given time step, the maximum gas velocity in this region and its position are determined. A homologous velocity $v(r) = \alpha r$ is then assigned to each grid point such that the velocity of the grid at the radius of maximum gas velocity in the outer 10% of the mesh is three times this maximum. The factor of 3 guarantees that the flow never reaches the outer edge of the grid, where boundary conditions are reset every time step to ensure that the SN always encounters the correct protogalactic density, as described above. A new radius is then computed for each grid point from its present radius, the velocity it is assigned from the homologous profile, and the current time step. This procedure preserves the total number of grid points and ensures that they are uniformly spaced between the new inner and outer boundaries.

3. EVOLUTION OF THE SN

3.1. Free Expansion

As the shock initially plows into the dense envelope it heats it to nearly 10^9 K, as we show in the left panel of Fig. 4. At these temperatures x-ray emission dominates

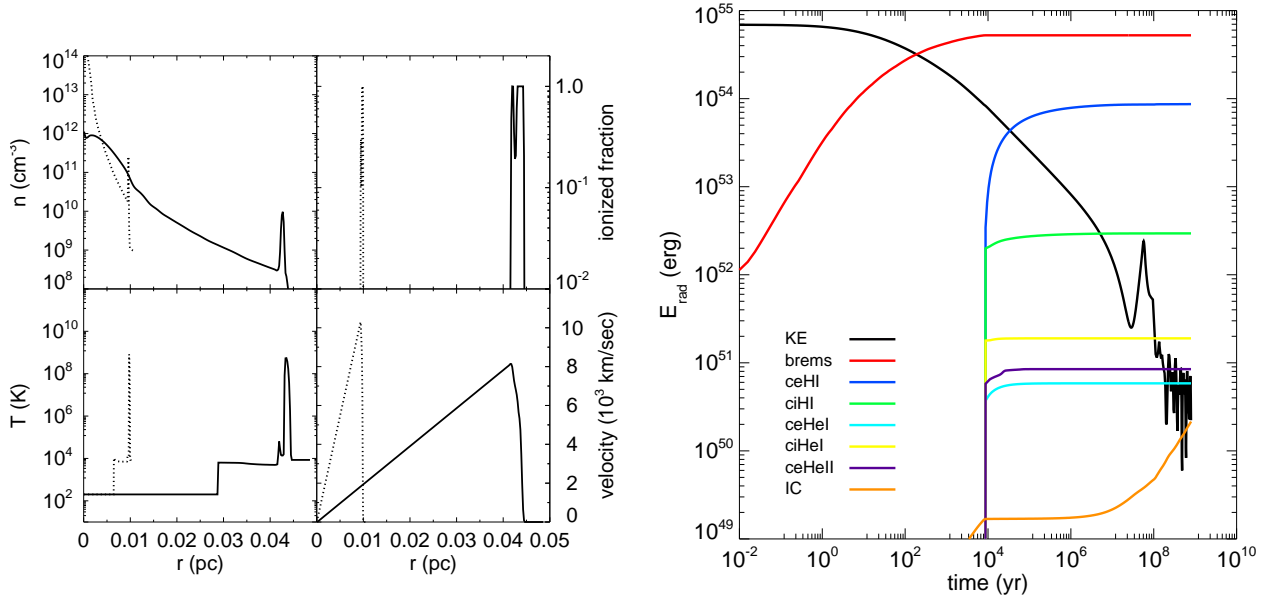


FIG. 4.— Left: The interaction of the free expansion with the dense protogalactic envelope. Dotted line: 0.658 yr. Solid line: 4.04 yr. Right: cumulative radiative losses from the SN remnant in the $4 \times 10^7 M_{\odot}$ protogalaxy versus time. KE is the kinetic energy of the remnant and the other plots are losses due to bremsstrahlung x-rays (brems), collisional excitation of H (ceHI), collisional ionization of H (ciHI), collisional excitation of He (ceHeI), collisional ionization of He (ciHeI), collisional excitation of He⁺ (ceHeII) and cooling due to upscattering of CMB photons (IC). Cooling due to collisional ionization of He⁺ is negligible and not shown.

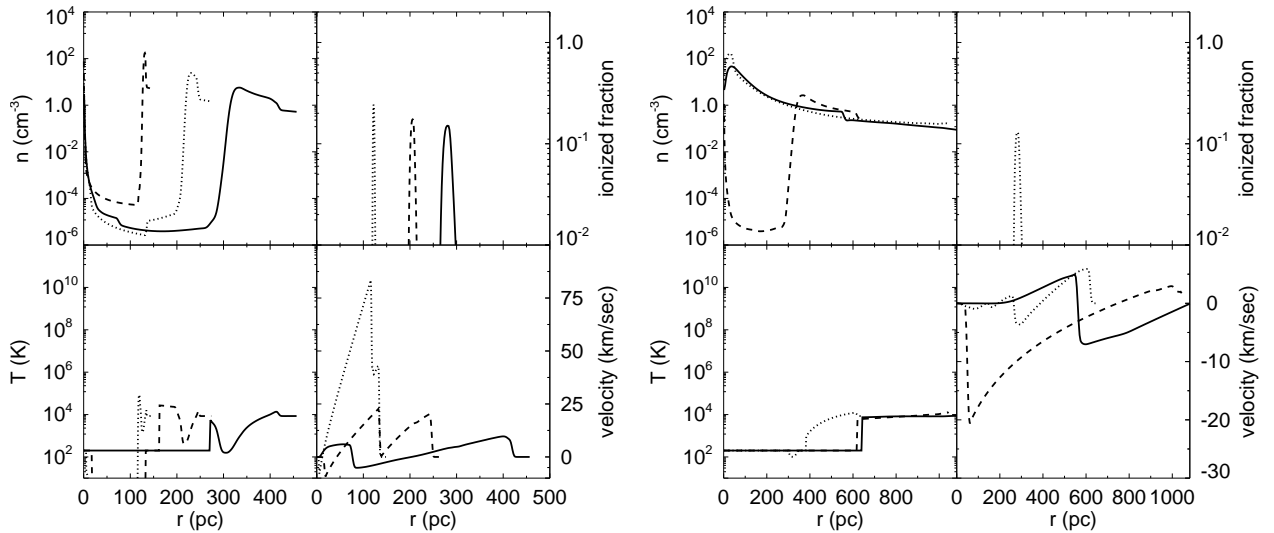


FIG. 5.— Left: Detachment of the reverse shock from the forward shock and its propagation into the interior of the remnant at 1.19 Myr (dashed line), 4.68 Myr (dotted line), and 13.5 Myr (solid line). Right: fallback into the protogalaxy. Dashed line: 26.2 Myr; dotted line: 58.7 Myr; solid line: 95.2 Myr.

energy losses from the shock and the ejecta rapidly loses energy, as shown in the right panel of Fig. 4. By $\sim 10^4$ yr bremsstrahlung losses have removed over 90% of the kinetic energy of the remnant. By this time the shock has cooled to $\sim 10^6$ K, and collisional excitation and ionization losses in H and He are activated in the gas. The shock cools to $\sim 10^4$ K in less than a Myr thereafter, because energy losses taper off by that time in Fig. 4. Losses by excitation and ionization of H and He in the shocked, swept-up gas eventually amount to $\sim 1\%$ of the original kinetic energy of the SN, with collisional excitation of H being the dominant cooling channel. During this time the remnant radiates large Ly- α fluxes.

3.2. Formation of the Reverse Shock / Onset of Mixing

As seen in the double peak in both ionization fractions and temperatures in Fig. 4, a reverse shock forms in the free expansion at early times but is not strong enough to fully detach from the forward shock or completely ionize the gas. It becomes stronger as the remnant sweeps up more of the halo, eventually heating to over 10^6 K and emitting large x-ray fluxes. The SN plows up approximately its own mass for each pc it expands in the halo, and when it reaches a radius of ~ 150 pc the reverse shock fully detaches from the forward shock and back-steps into the ejecta, as shown at 1.19 and 4.68 Myr in the left panel of Fig. 5. The forward shock decelerates from ~ 80 km s $^{-1}$ to 13 km s $^{-1}$.

The arrival of the reverse shock at the center of the halo and its subsequent rebound is visible in the velocity peak at ~ 75 pc at 13.5 Myr. By this stage the bulk of the remnant lies in a dense shell from 300 - 400 pc and it has evacuated the interior to very low densities. Essentially all radiative cooling has halted at this point because gas temperatures have fallen below 10^4 K everywhere, so the forward and reverse shocks now propagate adiabatically. We note that the retreat of the reverse shock through the dense ejecta shell would likely trigger Rayleigh-Taylor instabilities in three dimensions and mix metals with gas from the halo. Turbulent mixing driven by fallback and inflow from filaments would then further distribute metals throughout the interior of the protogalaxy at later times.

3.3. Fallback

By 26.2 Myr, when the remnant has grown to ~ 600 pc, the gravitational potential of the halo has halted its expansion, and all but its outermost layers fall back toward the center of the protogalaxy as shown in the right panel of Fig. 5. The reverse shock rebounding from the center of the protogalaxy collides with the inner surface of the collapsing shell and is again driven back into the center of the halo. This shock reverberates between the shell and the center of the protogalaxy with increasing frequency as the ejecta crushes the low-density cavity into the center of the halo. The shell reaches the center of the halo by 58.7 Myr, raising gas densities to ~ 200 cm $^{-3}$ there. As shown in Fig. 6, infall rates through the central 50 pc of the halo, as tallied by

$$\dot{m} = 4\pi r^2 \rho v_{\text{gas}}, \quad (3)$$

reach $\sim 1 M_{\odot} \text{ yr}^{-1}$ and persist for nearly 10^7 yr, so most of the baryons originally interior to the virial radius of

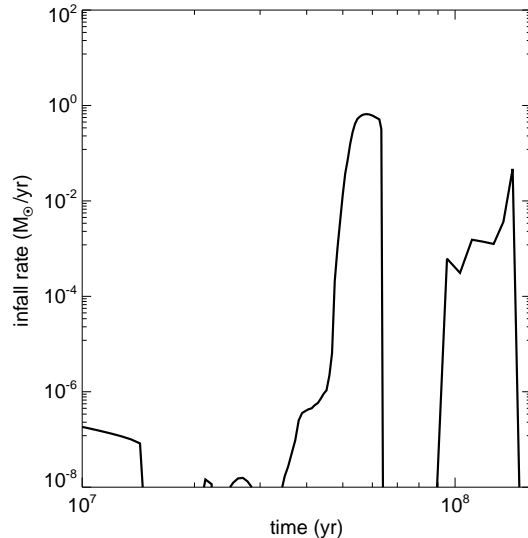


FIG. 6.— Accretion rates at the center of the $4 \times 10^7 M_{\odot}$ protogalaxy due to fallback. The first episode of fallback, from $5 - 6 \times 10^7$ yr, has the largest mass flux, $\sim 1 M_{\odot} \text{ yr}^{-1}$. Later bouts of accretion are due to subsequent cycles of adiabatic expansion and collapse of baryons in the halo.

the protogalaxy eventually fall to its center. Meanwhile, the momentum of the uppermost layers of the remnant lift the outer layers of the protogalaxy to altitudes of 1 - 1.5 kpc but they soon settle back down onto the halo.

After this first episode of fallback, the ejecta and baryons rebound adiabatically back out into the protogalaxy, as shown in Fig. 5 at 95.2 Myr. The leading edge of the outward flow is visible as the ripple in density and the velocity peak at ~ 600 pc. As the ejecta propagates outward, it again stalls in the DM potential of the halo and falls back toward the center. In our models this cycle continues for several hundred Myr and is manifest as the oscillations in KE at late times in the right panel of Fig. 4. In reality, accretion from filaments and mergers with other halos would disrupt this motion as they agitate gas at the center of the protogalaxy. Furthermore, departures from spherical symmetry in real protogalaxies, or off-center explosions, could allow more ejecta to flow out into the IGM, especially if UV flux from the SN progenitor opens channels of low column density out of the halo through which metals can escape. If metals and dust mix completely with the baryons in the halo, as our results suggest, the metallicity of the protogalaxy will abruptly rise to $0.1 Z_{\odot}$ after just one explosion in 50 - 100 Myr.

The fact that the protogalaxy traps most metals from explosions this energetic is counter to what might naively be expected from simple binding energy arguments. The binding energy E_B of the gas in the halo can be approximated by that of an isothermal sphere,

$$E_B = \int_0^{R_{\text{vir}}} \frac{GM_{\text{encl}}}{r} 4\pi r^2 \rho_B(r) dr, \quad (4)$$

where

$$M_{\text{encl}} = \int_0^r 4\pi r'^2 (\rho_{\text{DM}}(r') + \rho_B(r')) dr' \quad (5)$$

and

$$\rho_{\text{DM}} = \frac{\Omega_{\text{M}} - \Omega_{\text{B}}}{\Omega_{\text{B}}} \rho_{\text{B}}. \quad (6)$$

If we take $\Omega_{\text{M}} = 0.266$ and $\Omega_{\text{B}} = 0.0449$, set the virial radius R_{vir} of the halo to be 1 kpc, and use Equation 1 for ρ_{B} , we obtain $E_{\text{B}} \sim 8.5 \times 10^{53}$ erg, which far less than the energy of the SN. But the gas is not blown out of the protogalaxy because the ejecta loses $> 95\%$ of its kinetic energy to bremsstrahlung x-rays by the time it reaches 1% of the virial radius of the halo. In fact, after radiative losses the kinetic energy of the remnant is very close to the binding energy of the gas to the dark matter, and this is why it only expands to R_{vir} before falling back into the halo. The DM potential of the protogalaxy slows down the growth of the remnant, never allowing it to become a momentum conserving snowplow. The remnant retains far more of its energy in H II regions, and blows all the gas from the protogalaxy as shown by Johnson et al. (2012b).

We neglect cosmic ray emission from the remnant because the strengths of magnetic fields in $z \sim 15$ protogalaxies, or even the progenitor stars themselves, are not well constrained (although see Schober et al. 2012; Latif et al. 2013). But such emission would simply slow down the expansion of the SN, confining it to even smaller radii than those here. Likewise, non-equilibrium radiative cooling by metals in the ejecta, which also transports some internal energy out of the remnant, is not included in our simulations. Consequently, the final radii of the explosions in our models should be taken to be upper limits.

3.4. Supermassive Pop III SNe and the CMB

Inverse Compton losses from the remnant are modest, just 1% of those from 140 - 260 M_{\odot} pair-instability (PI) SNe in $z \sim 25$ minihalos (Whalen et al. 2008). In those explosions the shock remains hotter at large radii because they occur in H II regions, so CMB photons are upscattered with greater efficiency in their interiors. In the SNe in this study, IC losses are much lower because the remnant cools before enclosing large volumes of CMB photons. The losses are small at first but later grow as the shock reaches larger radii.

It is clear that supermassive explosions in H II regions in early protogalaxies would leave a larger imprint on the CMB via the Sunyayev-Zeldovich effect than the SNe in our models. Low explosion rates probably prevented such SNe from collectively imposing excess power on the CMB on small scales. However, unlike PI SNe at earlier epochs, these SN remnants may become large enough to be directly resolved by current instruments like the *Atacama Cosmology Telescope* (ACT) and the *South Pole Telescope* (SPT) in addition to being detected in the near infrared (NIR; Whalen et al. 2012b) by future missions such as the *Wide-Field Infrared Survey Telescope* (WFIRST) and the *Wide-Field Imaging Surveyor for High Redshift* (WISH). Calculations of the imprint of these and other types of Pop III SNe on the CMB are now underway.

3.5. SN in More Massive Halos

Explosions in H II regions in protogalaxies, as in Johnson et al. (2012b), can eventually range 10 kpc or

more from their host halos, perhaps even contaminating other nearby protogalaxies with metals. In contrast, SNe in undisturbed halos briefly engulf the protogalaxy but then collapse back into it, with few metals lost to the IGM. Our fiducial halo is on the low end of the mass scale for atomically cooled protogalaxies so explosions in more massive structures will be confined to even smaller radii, as we find for the SN in our $3.2 \times 10^8 M_{\odot}$ halo. This explosion evolves in basically the same manner as in the less massive halo but with two important differences.

First, because the shock initially plows into much higher densities it cools more quickly, radiating fewer x-rays and allowing H and He line cooling to activate at much earlier times. As we show in the right panel of Fig. 7, He line losses dominate cooling in the remnant rather than x-rays. Second, because the shock cools more rapidly the SN ejecta only expands to a radius of 80 pc before falling back into the halo. Consequently, this explosion will be less efficient at enriching gas in the protogalaxy although turbulent mixing by cosmological flows along filaments will still enhance this process. As shown in the right panel of Fig. 7, peak fallback rates in this protogalaxy are nearly ten times those in the less massive halo but last for only 2 Myr instead of 10 Myr. About the same amount of gas collapses back to the center of the halo in this first episode of fallback, fueling the rapid growth of any SMBH seeds there.

4. RADIO SIGNATURES OF SUPERMASSIVE POP III SNE

Shocks in SN remnants accelerate electrons to relativistic velocities, giving rise to radio synchrotron emission. We compute the emission spectrum of the SN in both protogalaxies, including both free-free and synchrotron radiation, as in Meiksin & Whalen (2013). Specifically, the electron distribution is taken to be a power law in energy $E = (\gamma - 1)m_e c^2$, $n(E) \propto E^{-p_e}$, with an average spectral index $p_e = 2$. Energy equipartition between the relativistic electrons and the magnetic field is assumed, allowing for a fraction $f_e = 0.01$ of the thermal energy to go into the relativistic electrons. The range in the relativistic γ factor is limited by post-shock energy losses, primarily plasmon excitation at the low energies and synchrotron cooling at high energies. Free-free absorption and synchrotron self-absorption are included.

The evolution of the spectrum of the SN in the lower-mass GADGET halo in the observer's frame for a source at $z = 15$ is shown in the left panel of Fig. 8 for several radio bands, including those accessible to the Square Kilometer Array⁶ (SKA) and ASKAP⁷. The peak radio fluxes are within the sensitivity range of the eVLA⁸ and eMERLIN⁹. The delay in the flux is due to the energy losses which pinch off the relativistic electron population at early times. Once the emission starts, the flux rises sharply, with a doubling time of months in the observer's frame. The flux is sharply peaked around 3 GHz during the rise, followed by radiation emerging at 1.4 GHz then 10 GHz. The signature is unusual and suggests an observing strategy of periodic surveys with observations carried out at intervals of several months to a few years,

⁶ www.skatelescope.org

⁷ www.atnf.csiro.au/projects/askap

⁸ www.aoc.nrao.edu/evla

⁹ www.jb.man.ac.uk/research/rflabs/eMERLIN.html

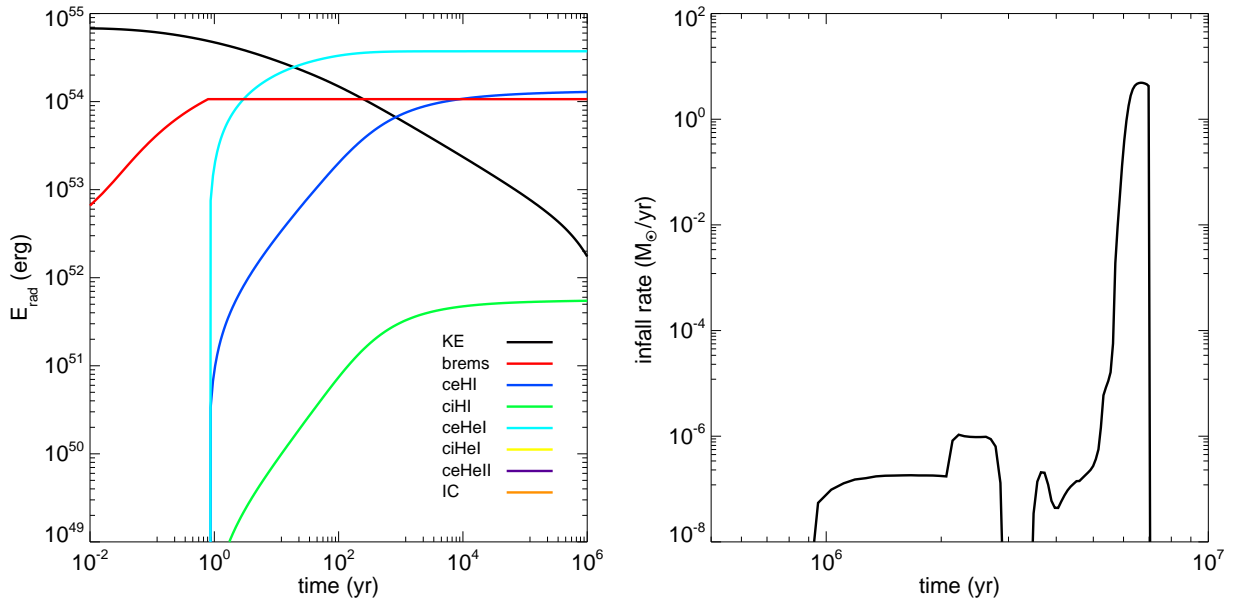


FIG. 7.— Left: cumulative radiative losses from the SN remnant in the $3.2 \times 10^8 M_{\odot}$ protogalaxy versus time. KE is the kinetic energy of the remnant and the other plots are losses due to bremsstrahlung x-rays (brems), collisional excitation of H (ceHI), collisional ionization of H (ciHI), collisional excitation of He (ceHeI), collisional ionization of He (ciHeI), collisional excitation of He⁺ (ceHeII) and cooling due to upscattering of CMB photons (IC). Cooling due to ciHeII, ceHeII, and IC are negligible and not shown. Right: infall rates at the center of the $3.2 \times 10^8 M_{\odot}$ protogalaxy due to fallback.

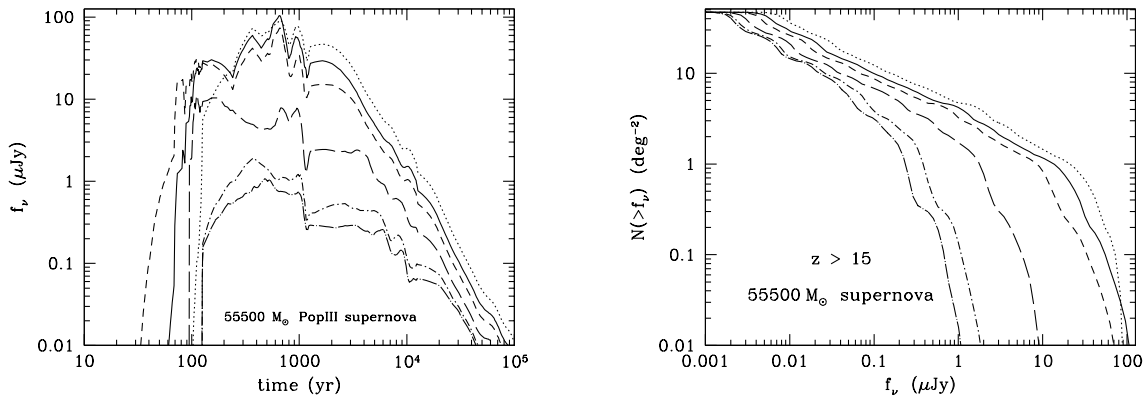


FIG. 8.— Left: radio light curves for a remnant in a $4 \times 10^7 M_{\odot}$ halo at $z = 15$ (observer's frame). The curves correspond to the bands: 0.5 (dotted), 1.4 (solid), 3 (short-dashed), 10 (long-dashed), 25 (dot short-dashed) and 35 (dot long-dashed) GHz. Right: the corresponding number counts above a given observed flux, assuming one SN per halo (the counts must be scaled down proportionately for lower supermassive SN rates).

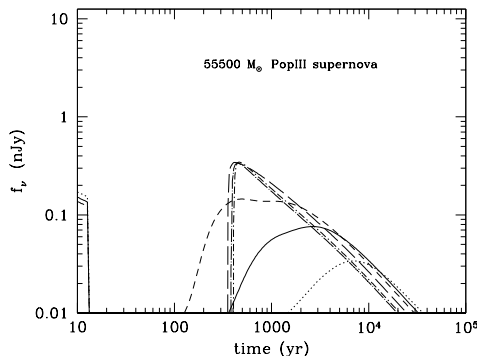


FIG. 9.— Radio light curves for the supermassive SN in a $3.2 \times 10^8 M_{\odot}$ halo at $z = 15$ (observer’s frame). The curves correspond to the bands: 0.5 (dotted), 1.4 (solid), 3 (short-dashed), 10 (long-dashed), 25 (dot short-dashed) and 35 (dot long-dashed) GHz.

searching for such narrowly peaked evolving sources. At late times, the source is red in the radio with most of the flux at the lower frequency of 500 MHz and falling sharply at frequencies above 3 GHz due to strong synchrotron losses.

The expected flux counts for the radio remnant are shown in the right panel of Fig. 8, assuming one SN per halo more massive than $4 \times 10^7 M_{\odot}$ (the numbers would have to be reduced proportionately for fewer SNe per halo.) Several sources brighter than $1 \mu\text{Jy}$ at frequencies below 10 GHz would be visible in a square degree field. However, we find that the radio signature of the explosion in the more massive *Enzo* protogalaxy is much dimmer, as we show in Fig. 9. This is due to the fact that the shock is cooler in the higher densities of the more massive halo because of the much higher recombination rates. As a result, such explosions emit far less synchrotron radiation and will not be visible even to SKA.

The long lifetimes of the remnants offer the possibility of detecting their 21 cm signature against a bright background radio source. While absorption from halos is predicted from cosmological structure formation, the signal from a given halo is a single absorption feature (although sometimes a doubly troughed blend) (Meiksin 2011). As shown in Fig. 10, the expansion of the SN remnant produces two distinct absorption troughs along lines of sight over a wide range in radii ($\sim 100 - 300$ pc), which persist for $\sim 10^7$ yr before merging into a single feature. Such a unique signature would distinguish halos with such powerful SNe from more quiescent ones. Assuming one such SN per halo, the number of such absorption features per redshift at $z > 15$ against a bright background radio source is $dN/dz \sim 0.0001 - 0.001$, much higher than the frequency found for much lower-mass SN progenitors (Meiksin & Whalen 2013). It is possible that sufficient numbers of bright radio sources exist at these redshifts to allow the detection of the features. The detection rate would be proportionately smaller for fewer SNe per halo.

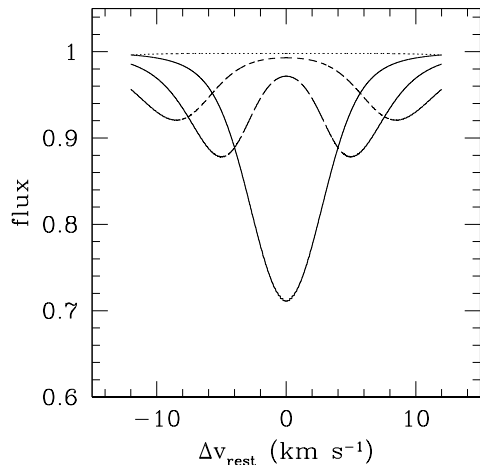


FIG. 10.— The 21 cm absorption signal against a bright background radio source for a remnant in a $4 \times 10^7 M_{\odot}$ halo at $z = 15$. The curves correspond to lines of sight following the expansion of the remnant, with an impact parameter from the center of the halo of $b_{\perp} = 110$ pc at 1.2 Myr after detonation (dotted line), $b_{\perp} = 200$ pc at 4.7 Myr (short-dashed line), $b_{\perp} = 240$ pc at 7.1 Myr (long-dashed line) and $b_{\perp} = 330$ pc at 13.5 Myr (solid line).

5. CONCLUSION

Supermassive Pop III SNe in dense halos briefly engulf the entire protogalaxy but then fall back into it in a spectacular manner, promptly enriching it to high metallicities. Subsequent mergers with other halos and cold accretion flows into the center of the protogalaxy further mix these metals throughout its interior. Metals radically alter cooling in the halo in spite of the LW background, potentially fragmenting a large fraction of its baryons into dense clumps and igniting a brilliant starburst. These bursts of early star formation would have lit up the early cosmos, creating large H II regions (Wise & Cen 2009) and driving strong winds into the IGM (Mac Low & Ferrara 1999; Fujita et al. 2004). Indeed, by triggering such starbursts supermassive Pop III SNe may have been drivers of early reionization. These bursts would also have created stellar populations that easily distinguished these special galaxies from others at the same redshift because their luminosities and metallicities would be greater than those of their more slowly evolving neighbors.

We note that these explosions could not have been studied in our previous work (Johnson et al. 2013b) because at early stages, when the SN remnant loses most of its energy, x-ray and line cooling timescales are ~ 100 s, far too short to be tractable in 3D. However, by the time the SN has lost most of its energy and its cooling times have become large, its radius in both halos is less than ~ 30 pc. At this radius, departures from spherical symmetry in the halo would not have imparted significant asymmetries to the ejecta and Rayleigh-Taylor instabilities due to reverse shocks would not have had time to form. It is therefore possible to initialize these explosions in 3D codes at later times to study their evolution in cosmological flows, having properly determined their energy and momentum losses up to that point. Fall-

back, prompt chemical enrichment and starbursts in LW protogalaxies in such flows are now being explored in GADGET (Johnson et al. 2013a).

The implications of primeval starbursts for the nucleosynthetic imprint of early SNe on the first galaxies (Cooke et al. 2011; Frebel & Bromm 2012) and on ancient, dim metal-poor stars (Beers & Christlieb 2005; Frebel et al. 2005; Cayrel et al. 2004; Lai et al. 2008; Caffau et al. 2012; Ren et al. 2012), remain unclear. Thermonuclear yields for supermassive Pop III SNe have only begun to be examined and may vary strongly with progenitor mass and explosion energy. A single massive explosion would also have enriched the entire protogalaxy to metallicities above those targeted by surveys of metal poor stars to date (Karlsson et al. 2008). Such galaxies would therefore have eluded discovery in the fossil record thus far. Elemental yields for supermassive Pop III SNe will be the focus of future simulation campaigns in order to reconcile them with coming observations.

Massive fallback may also have fueled the rapid growth of $10^4 - 10^6 M_{\odot}$ BHs from other supermassive clumps that formed from atomic cooling in the halo. As shown in Fig. 6, fallback rates at the center of the protogalaxy can be as high as $1 M_{\odot} \text{ yr}^{-1}$ for up to 10^7 Myr, perhaps driving BH accretion rates above the Eddington limit there.

Although these infall rates are high, they are also intermittent, so it is not yet known how quickly the BHs can acquire mass. How x-ray feedback from the BH regulates fallback is also unknown. Nevertheless, given these uncertainties it is still likely that these BHs, which might be the seeds of SMBHs, will have episodes of rapid and perhaps super-Eddington growth. High-redshift protogalaxies with star formation rates much higher than those of other halos of similar mass, along with detections of the most energetic SNe in the universe in the NIR, radio and CMB, may soon mark the birthplaces of SMBHs on the sky.

DJW acknowledges support from the Baden-Württemberg-Stiftung by contract research via the programme Internationale Spitzenforschung II (grant P-LS-SPII/18). JLJ and JS were supported by LANL Director's Fellowships. Work at LANL was done under the auspices of the National Nuclear Security Administration of the U.S. Department of Energy at Los Alamos National Laboratory under Contract No. DE-AC52-06NA25396. All ZEUS-MP simulations were performed on Institutional Computing platforms (Pinto) at LANL.

REFERENCES

- Abel, T., Anninos, P., Zhang, Y., & Norman, M. L. 1997, *New Astronomy*, 2, 181
- Abel, T., Bryan, G. L., & Norman, M. L. 2000, *ApJ*, 540, 39 —. 2002, *Science*, 295, 93
- Abel, T., Wise, J. H., & Bryan, G. L. 2007, *ApJ*, 659, L87
- Agarwal, B., Khochfar, S., Johnson, J. L., Neistein, E., Dalla Vecchia, C., & Livio, M. 2012, *MNRAS*, 425, 2854
- Alvarez, M. A., Bromm, V., & Shapiro, P. R. 2006, *ApJ*, 639, 621
- Alvarez, M. A., Wise, J. H., & Abel, T. 2009, *ApJ*, 701, L133
- Anninos, P., Zhang, Y., Abel, T., & Norman, M. L. 1997, *New Astronomy*, 2, 209
- Appenzeller, I. & Fricke, K. 1972a, *A&A*, 18, 10
- . 1972b, *A&A*, 21, 285
- Beers, T. C. & Christlieb, N. 2005, *ARA&A*, 43, 531
- Begelman, M. C. 2010, *MNRAS*, 402, 673
- Begelman, M. C., Volonteri, M., & Rees, M. J. 2006, *MNRAS*, 370, 289
- Bond, J. R., Arnett, W. D., & Carr, B. J. 1984, *ApJ*, 280, 825
- Bromm, V., Coppi, P. S., & Larson, R. B. 1999, *ApJ*, 527, L5
- . 2002, *ApJ*, 564, 23
- Bromm, V. & Loeb, A. 2003, *ApJ*, 596, 34
- Bryan, G. L. & Norman, M. L. 1997, *ArXiv Astrophysics e-prints*
- Bryan, G. L., Norman, M. L., Stone, J. M., Cen, R., & Ostriker, J. P. 1995, *Computer Physics Communications*, 89, 149
- Caffau, E., Bonifacio, P., François, P., Spite, M., Spite, F., Zaggia, S., Ludwig, H.-G., Steffen, M., Mashonkina, L., Monaco, L., Sbordone, L., Molaro, P., Cayrel, R., Plez, B., Hill, V., Hammer, F., & Randich, S. 2012, *A&A*, 542, A51
- Cayrel, R., Depagne, E., Spite, M., Hill, V., Spite, F., François, P., Plez, B., Beers, T., Primas, F., Andersen, J., Barbuy, B., Bonifacio, P., Molaro, P., & Nordström, B. 2004, *A&A*, 416, 1117
- Cherchneff, I. & Dwek, E. 2009, *ApJ*, 703, 642
- . 2010, *ApJ*, 713, 1
- Cherchneff, I. & Lilly, S. 2008, *ApJ*, 683, L123
- Chiaki, G., Yoshida, N., & Kitayama, T. 2013, *ApJ*, 762, 50
- Clark, P. C., Glover, S. C. O., Smith, R. J., Greif, T. H., Klessen, R. S., & Bromm, V. 2011, *Science*, 331, 1040
- Cooke, R., Pettini, M., Steidel, C. C., Rudie, G. C., & Jorgenson, R. A. 2011, *MNRAS*, 412, 1047
- Couchman, H. M. P. 1991, *ApJ*, 368, L23
- de Souza, R. S., Ishida, E. E. O., Johnson, J. L., Whalen, D. J., & Mesinger, A. 2013, *arXiv:1306.4984*
- de Souza, R. S., Rodrigues, L. F. S., Ishida, E. E. O., & Opher, R. 2011, *MNRAS*, 415, 2969
- Dessart, L., Waldman, R., Livne, E., Hillier, D. J., & Blondin, S. 2013, *MNRAS*, 428, 3227
- Dijkstra, M., Haiman, Z., Mesinger, A., & Wyithe, J. S. B. 2008, *MNRAS*, 391, 1961
- Djorgovski, S. G., Volonteri, M., Springel, V., Bromm, V., & Meylan, G. 2008, in *The Eleventh Marcel Grossmann Meeting On Recent Developments in Theoretical and Experimental General Relativity, Gravitation and Relativistic Field Theories*, ed. H. Kleinert, R. T. Jantzen, & R. Ruffini, 340–367
- Dwek, E. & Cherchneff, I. 2011, *ApJ*, 727, 63
- Efstathiou, G., Davis, M., White, S. D. M., & Frenk, C. S. 1985, *ApJS*, 57, 241
- Fan, X., Strauss, M. A., Richards, G. T., Hennawi, J. F., Becker, R. H., White, R. L., Diamond-Stanic, A. M., Donley, J. L., Jiang, L., Kim, J. S., Vestergaard, M., Young, J. E., Gunn, J. E., Lupton, R. H., Knapp, G. R., Schneider, D. P., Brandt, W. N., Bahcall, N. A., Barentine, J. C., Brinkmann, J., Brewington, H. J., Fukugita, M., Harvanek, M., Kleinman, S. J., Krzesinski, J., Long, D., Neilsen, Jr., E. H., Nitta, A., Snedden, S. A., & Voges, W. 2006, *AJ*, 131, 1203
- Fan, X., Strauss, M. A., Schneider, D. P., Becker, R. H., White, R. L., Haiman, Z., Gregg, M., Pentericci, L., Grebel, E. K., Narayanan, V. K., Loh, Y., Richards, G. T., Gunn, J. E., Lupton, R. H., Knapp, G. R., Ivezić, Ž., Brandt, W. N., Collinge, M., Hao, L., Harbeck, D., Prada, F., Schaye, J., Strateva, I., Zakamska, N., Anderson, S., Brinkmann, J., Bahcall, N. A., Lamb, D. Q., Okamura, S., Szalay, A., & York, D. G. 2003, *AJ*, 125, 1649
- Fowler, W. A. 1966, *ApJ*, 144, 180
- Fowler, W. A. & Hoyle, F. 1964, *ApJS*, 9, 201
- Frebel, A., Aoki, W., Christlieb, N., Ando, H., Asplund, M., Barklem, P. S., Beers, T. C., Eriksson, K., Fechner, C., Fujimoto, M. Y., Honda, S., Kajino, T., Minezaki, T., Nomoto, K., Norris, J. E., Ryan, S. G., Takada-Hidai, M., Tsangarides, S., & Yoshii, Y. 2005, *Nature*, 434, 871
- Frebel, A. & Bromm, V. 2012, *ApJ*, 759, 115
- Frey, L. H., Even, W., Whalen, D. J., Fryer, C. L., Hungerford, A. L., Fontes, C. J., & Colgan, J. 2013, *ApJS*, 204, 16
- Fryer, C. L., Whalen, D. J., & Frey, L. 2010, in *American Institute of Physics Conference Series*, Vol. 1294, American Institute of Physics Conference Series, ed. D. J. Whalen, V. Bromm, & N. Yoshida, 70–75

- Fujita, A., Mac Low, M.-M., Ferrara, A., & Meiksin, A. 2004, *ApJ*, 613, 159
- Fuller, G. M., Woosley, S. E., & Weaver, T. A. 1986, *ApJ*, 307, 675
- Gall, C., Hjorth, J., & Andersen, A. C. 2011, *A&A Rev.*, 19, 43
- Gittings, M., Weaver, R., Clover, M., Betlach, T., Byrne, N., Coker, R., Dendy, E., Hueckstaedt, R., New, K., Oakes, W. R., Ranta, D., & Stefan, R. 2008, *Computational Science and Discovery*, 1, 015005
- Greif, T. H., Bromm, V., Clark, P. C., Glover, S. C. O., Smith, R. J., Klessen, R. S., Yoshida, N., & Springel, V. 2012, *MNRAS*, 424, 399
- Greif, T. H., Glover, S. C. O., Bromm, V., & Klessen, R. S. 2010, *ApJ*, 716, 510
- Greif, T. H., Johnson, J. L., Klessen, R. S., & Bromm, V. 2008, *MNRAS*, 387, 1021
- Greif, T. H., Springel, V., White, S. D. M., Glover, S. C. O., Clark, P. C., Smith, R. J., Klessen, R. S., & Bromm, V. 2011, *ApJ*, 737, 75
- Hahn, O. & Abel, T. 2011, *MNRAS*, 415, 2101
- Heger, A. & Chen, K.-J. 2013, *ApJ*, in prep
- Hummel, J. A., Pawlik, A. H., Milosavljević, M., & Bromm, V. 2012, *ApJ*, 755, 72
- Iben, Jr., I. 1963, *ApJ*, 138, 1090
- Jeon, M., Pawlik, A. H., Greif, T. H., Glover, S. C. O., Bromm, V., Milosavljević, M., & Klessen, R. S. 2012, *ApJ*, 754, 34
- Joggerst, C. C., Almgren, A., Bell, J., Heger, A., Whalen, D., & Woosley, S. E. 2010, *ApJ*, 709, 11
- Joggerst, C. C. & Whalen, D. J. 2011, *ApJ*, 728, 129
- Johnson, J. L. & Bromm, V. 2007, *MNRAS*, 374, 1557
- Johnson, J. L., Greif, T. H., & Bromm, V. 2008, *MNRAS*, 388, 276
- Johnson, J. L., Greif, T. H., Bromm, V., Klessen, R. S., & Ippolito, J. 2009, *MNRAS*, 399, 37
- Johnson, J. L., Khochfar, S., Greif, T. H., & Durier, F. 2011, *MNRAS*, 410, 919
- Johnson, J. L., Whalen, D. J., Even, W., Fryer, C. L., Heger, A., & Chen, K.-J. 2013a, *ApJ*, in prep
- Johnson, J. L., Whalen, D. J., Even, W., Fryer, C. L., Heger, A., Smidt, J., & Chen, K.-J. 2013b, *arXiv:1304.4601*
- Johnson, J. L., Whalen, D. J., Fryer, C. L., & Li, H. 2012a, *ApJ*, 750, 66
- Johnson, J. L., Whalen, D. J., Li, H., & Holz, D. E. 2012b, *arXiv:1211.0548*
- Karlsson, T., Johnson, J. L., & Bromm, V. 2008, *ApJ*, 679, 6
- Kasen, D., Woosley, S. E., & Heger, A. 2011, *ApJ*, 734, 102
- Kitayama, T. & Yoshida, N. 2005, *ApJ*, 630, 675
- Kitayama, T., Yoshida, N., Susa, H., & Umemura, M. 2004, *ApJ*, 613, 631
- Komatsu, E., Smith, K. M., Dunkley, J., Bennett, C. L., Gold, B., Hinshaw, G., Jarosik, N., Larson, D., Nolte, M. R., Page, L., Spergel, D. N., Halpern, M., Hill, R. S., Kogut, A., Limon, M., Meyer, S. S., Odegard, N., Tucker, G. S., Weiland, J. L., Wollack, E., & Wright, E. L. 2011, *ApJS*, 192, 18
- Lai, D. K., Bolte, M., Johnson, J. A., Lucatello, S., Heger, A., & Woosley, S. E. 2008, *ApJ*, 681, 1524
- Latif, M. A., Schleicher, D. R. G., Schmidt, W., & Niemeyer, J. 2013, *MNRAS*
- Lippai, Z., Frei, Z., & Haiman, Z. 2009, *ApJ*, 701, 360
- Mac Low, M.-M. & Ferrara, A. 1999, *ApJ*, 513, 142
- Mackey, J., Bromm, V., & Hernquist, L. 2003, *ApJ*, 586, 1
- Meiksin, A. 2011, *MNRAS*, 417, 1480
- Meiksin, A. & Whalen, D. J. 2013, *MNRAS*, 430, 2854
- Milosavljević, M., Bromm, V., Couch, S. M., & Oh, S. P. 2009, *ApJ*, 698, 766
- Montero, P. J., Janka, H.-T., & Müller, E. 2012, *ApJ*, 749, 37
- Mortlock, D. J., Warren, S. J., Venemans, B. P., Patel, M., Hewett, P. C., McMahon, R. G., Simpson, C., Theuns, T., González-Solares, E. A., Adamson, A., Dye, S., Hambly, N. C., Hirst, P., Irwin, M. J., Kuiper, E., Lawrence, A., & Röttgering, H. J. A. 2011, *Nature*, 474, 616
- Nakamura, F. & Umemura, M. 2001, *ApJ*, 548, 19
- O’Shea, B. W., Bryan, G., Bordner, J., Norman, M. L., Abel, T., Harkness, R., & Kritsuk, A. 2004, *ArXiv Astrophysics e-prints*
- O’Shea, B. W. & Norman, M. L. 2007, *ApJ*, 654, 66
- 2008, *ApJ*, 673, 14
- Pan, T., Kasen, D., & Loeb, A. 2012a, *MNRAS*, 422, 2701
- Pan, T., Loeb, A., & Kasen, D. 2012b, *MNRAS*, 423, 2203
- Park, K. & Ricotti, M. 2011, *ApJ*, 739, 2
- 2012a, *ApJ*, 747, 9
- 2012b, *arXiv:1211.0542*
- Pawlik, A. H., Milosavljević, M., & Bromm, V. 2011, *ApJ*, 731, 54
- 2013, *ApJ*, 767, 59
- Petri, A., Ferrara, A., & Salvaterra, R. 2012, *MNRAS*, 422, 1690
- Regan, J. A. & Haehnelt, M. G. 2009, *MNRAS*, 396, 343
- Ren, J., Christlieb, N., & Zhao, G. 2012, *Research in Astronomy and Astrophysics*, 12, 1637
- Ritter, J. S., Safraneck-Shrader, C., Gnat, O., Milosavljević, M., & Bromm, V. 2012, *ApJ*, 761, 56
- Scannapieco, E., Madau, P., Woosley, S., Heger, A., & Ferrara, A. 2005, *ApJ*, 633, 1031
- Schober, J., Schleicher, D., Federrath, C., Glover, S., Klessen, R. S., & Banerjee, R. 2012, *ApJ*, 754, 99
- Shang, C., Bryan, G. L., & Haiman, Z. 2010, *MNRAS*, 402, 1249
- Smith, B. D. & Sigurdsson, S. 2007, *ApJ*, 661, L5
- Smith, B. D., Turk, M. J., Sigurdsson, S., O’Shea, B. W., & Norman, M. L. 2009, *ApJ*, 691, 441
- Smith, R. J., Glover, S. C. O., Clark, P. C., Greif, T., & Klessen, R. S. 2011, *MNRAS*, 414, 3633
- Springel, V. & Hernquist, L. 2002, *MNRAS*, 333, 649
- Springel, V., Yoshida, N., & White, S. D. M. 2001, *New Astronomy*, 6, 79
- Stacy, A., Greif, T. H., & Bromm, V. 2010, *MNRAS*, 403, 45
- Tanaka, T. & Haiman, Z. 2009, *ApJ*, 696, 1798
- Toro, E. F., Spruce, M., & Speares, W. 1994, *Shock Waves*, 4, 25
- Truelove, J. K., Klein, R. I., McKee, C. F., Holliman, II, J. H., Howell, L. H., & Greenough, J. A. 1997, *ApJ*, 489, L179
- Turk, M. J., Abel, T., & O’Shea, B. 2009, *Science*, 325, 601
- Vasiliev, E. O., Vorobyov, E. I., Matvienko, E. E., Razoumov, A. O., & Shchekinov, Y. A. 2012, *Astronomy Reports*, 56, 895
- Weaver, T. A., Zimmerman, G. B., & Woosley, S. E. 1978, *ApJ*, 225, 1021
- Whalen, D., Abel, T., & Norman, M. L. 2004, *ApJ*, 610, 14
- Whalen, D. & Norman, M. L. 2006, *ApJS*, 162, 281
- 2008a, *ApJ*, 673, 664
- Whalen, D., van Veelen, B., O’Shea, B. W., & Norman, M. L. 2008, *ApJ*, 682, 49
- Whalen, D. J., Even, W., Frey, L. H., Johnson, J. L., Lovekin, C. C., Fryer, C. L., Stiavelli, M., Holz, D. E., Heger, A., Woosley, S. E., & Hungerford, A. L. 2012a, *arXiv:1211.4979*
- Whalen, D. J., Even, W., Lovekin, C. C., Fryer, C. L., Stiavelli, M., Roming, P. W. A., Cooke, J., Pritchard, T. A., Holz, D. E., & Knight, C. 2013a, *arXiv:1302.0436*
- Whalen, D. J. & Fryer, C. L. 2012, *ApJ*, 756, L19
- Whalen, D. J., Fryer, C. L., Holz, D. E., Heger, A., Woosley, S. E., Stiavelli, M., Even, W., & Frey, L. H. 2013b, *ApJ*, 762, L6
- Whalen, D. J., Heger, A., Chen, K.-J., Even, W., Fryer, C. L., Stiavelli, M., Xu, H., & Joggerst, C. C. 2012b, *arXiv:1211.1815*
- Whalen, D. J., Joggerst, C. C., Fryer, C. L., Stiavelli, M., Heger, A., & Holz, D. E. 2012c, *arXiv:1209.5459*
- Whalen, D. J. & Norman, M. L. 2008b, *ApJ*, 672, 287
- Willott, C. J., McLure, R. J., & Jarvis, M. J. 2003, *ApJ*, 587, L15
- Wise, J. H. & Abel, T. 2007, *ApJ*, 671, 1559
- 2008, *ApJ*, 684, 1
- Wise, J. H. & Cen, R. 2009, *ApJ*, 693, 984
- Wise, J. H., Turk, M. J., & Abel, T. 2008, *ApJ*, 682, 745
- Wise, J. H., Turk, M. J., Norman, M. L., & Abel, T. 2012, *ApJ*, 745, 50
- Wolcott-Green, J., Haiman, Z., & Bryan, G. L. 2011, *MNRAS*, 418, 838
- Woodward, P. & Colella, P. 1984, *Journal of Computational Physics*, 54, 115
- Woosley, S. E., Heger, A., & Weaver, T. A. 2002, *Reviews of Modern Physics*, 74, 1015
- Yoshida, N., Omukai, K., & Hernquist, L. 2008, *Science*, 321, 669